

THEORETICAL DIFFRACTIVE FILTER PERFORMANCE FOR BALLISTIC TRANSILLUMINATION

Paulino Vacas-Jacques¹ (D.Sc. aspirant, e-mail: pvj@cio.mx),

Vladimir Ryabukho^{2,3} (professor, e-mail: rvp@sgu.ru),

Marija Strojnik¹ (professor, e-mail: mstrojnik@aol.com),

Valery Tuchin^{2,3} (head of chair, professor, e-mail: tuchin@sgu.ru),

Gonzalo Paez¹ (professor, e-mail: gpaez@cio.mx)

¹ *Centro de Investigaciones en Optica, 37000, Leon, Guanajuato, Mexico*

² *Saratov State University, 410012, Saratov, Russia*

³ *Institute of Precision Mechanics and Control of the Russian Academy of Sciences, 410028, Saratov, Russia*

Abstract

We address the topic of selectively probing turbid media, equivalent to biological tissue, with ballistic photons. The samples considered exhibit highly forward-directed scattering (anisotropy factor $g > 0.9$). We propose the utilization of a non-linear grating-based angular filter to separate the faint ballistic signal from optical noise. The filter is conformed of a monochromatic source incident on a ruled grating, positioned at grazing diffraction, followed by a narrow slit. Minute deviations in propagation angle of scattered radiation are amplified non-linearly. A rotation scheme with 1 arc min resolution may provide angular amplifications in the range of 15X-60X. In addition, similar values of transversal beam size reduction enable efficient ~100X-1000X filtering of optical noise. We utilize random walk Monte Carlo calculations to emulate the interactions between radiation and turbid media. The influence of the filter is considered by employing ray trace analysis and conical diffraction theory of ruled gratings. For samples with $g \leq 0.99$, we demonstrate that the filter enables isolation of ballistic photons. For very marked forward-scattering $g \geq 0.995$, the configuration permits a significant $\sim 10^3$ reduction of optical noise.

Key words: Angular filter, grazing diffraction, ruled gratings, conical diffraction, Monte Carlo computations, ballistic transillumination, tissue imaging, tissue characterization.

Introduction

During the last decades, a growing interest in the application of novel optical techniques to solve biomedical problems has ensued. Currently, a paradigm shift is taking place in the management of dental caries. The tendency is to enhance the diagnosis of early non-cavitated lesions. The expected outcome of this initiative is the proposal of innovative strategies for prevention and arrest of dental decay [1].

Early dental lesions manifest as a demineralization of enamel tissue. In addition, sound enamel is rather transparent to infrared radiation. In contrast, enamel with early lesions may attenuate radiation markedly [2]. Thus, in our group, we have proposed to use the decrease in ballistic transmission for characterization and imaging of enamel-like samples. In the technique, we employ an interferometric setup in cross-correlation modality [3,4].

Recently, we have developed an auto-correlation interferometer for studying biological samples in reflection geometry [5,6]. Furthermore, we are interested in proposing a transmission, or transillumination, interferometric setup in auto-correlation modality. In Fig. 1, we depict a schematic of such technique.

In our proposal, we are mainly interested in ballistic light. Quantitative and qualitative information of, for instance, dental decay may ensue from variations in ballistic transmittance. However, the intricate behavior of light in turbid media, such as enamel, complicates considerably the use of ballistic photons. The latter are always accompanied and obscured by forward-scattered contributions.

In fact, transmission of light in a turbid medium is governed by the radiative transport equation [7-10]. Furthermore, the attenuation characteristics of the media are required to describe the propagation of radiation. More specifically, the necessary parameters are the absorption coefficient μ_a [mm^{-1}], the scattering coefficient μ_s [mm^{-1}], and the anisotropy factor g . The first two values describe the probability of absorption and scattering per unit length. The third parameter determines the average direction of propagation after interaction.

Mathematically, $g = \int_{-1}^1 S(\theta) \cos \theta d(\cos \theta)$. The phase function $S(\theta)$ accounts for the angular pattern of scattering in the medium, and θ is the angle between incident and scattered directions. Biological tissues commonly exhibit phase functions with marked forward-directed patterns [11,12].

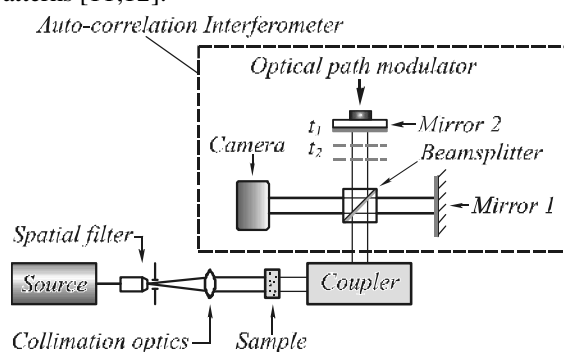


Fig. 1. Scheme of an auto-correlation interferometer in transillumination modality

One of the challenges in the implementation of a transillumination technique with ballistic photons resides in the rapid attenuation of such radiation. A perhaps more complicated endeavor however, is the separation of ballistic photons from those that have undergone scattering. The latter assertion is further validated by recognizing that the anisotropy factor is usually greater than 0.9 for biological tissues [13].

As an illustrative example, in Fig. 2 we show the mingled presence of ballistic and scattered photons as the anisotropy varies. The diameter of the beam is 12 mm, a consistent value with the size of dental tissues. Sample thickness is 10 mm; $\mu_a = 0$ [mm^{-1}], $\mu_s = 0.591$ [mm^{-1}], and $g = \{0.93, 0.99, 0.995\}$. Each number on the upper left corner of Fig. 2 corresponds to a greater value of g .

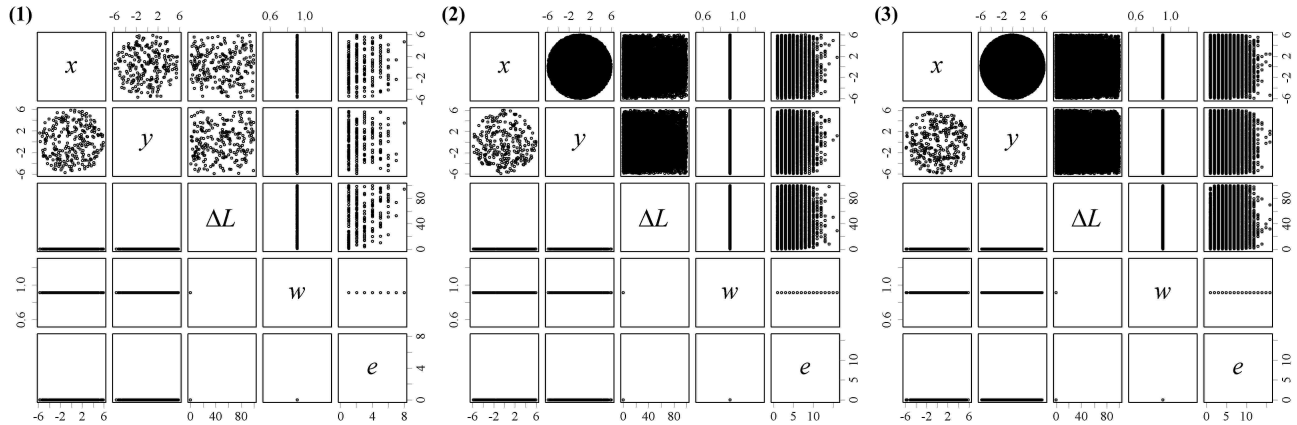


Fig. 2. Commingled presence of ballistic and scattered radiation after transillumination; (1) $g = 0.93$, (2) $g = 0.99$, and (3) $g = 0.995$

Data below and above the main diagonal, in Fig. 2, correspond to that of ballistic and scattered photons. Each row-column intersection is a scatter plot of the associated variables in the diagonal. x and y correspond to transversal coordinates in millimeters. ΔL stands for optical path-length difference in microns. w is weight or significance, and e represents the number of scattering events. Variables w and e are dimensionless.

The distinct scenarios in Fig. 2 serve to mimic the behavior of dental decay in enamel. A decrease in the value of the anisotropy factor could imply that the tissue is experiencing entropy. High values of the anisotropy factor have been reported to be characteristic of sound enamel, $g = 0.96$. Meanwhile, demineralized enamel exhibits a less structured composition, which in turn reflects as a variation in the scattering pattern [14].

In Fig. 2, the theoretical transversal distributions (x vs y) of scattered and ballistic photons, after transillumination, yield important insight. Information of scattered photons is found in the first row and second column intersection. Ballistic data is located in the second row and first column. Clearly, ballistic and scattered photons coexist, which raises a caveat for the implementation of the auto-correlation interferometer of Fig. 1. A method is required to distinguish ballistic from forward-scattered photons.

In addition, from the figure we may identify the major competing process in the transillumination procedure. For this purpose, we analyze the weight to number of events plot for scattered photons. Such information is found in the fourth row and fifth column intersection. For simplicity, we examine the data of scenario (1). From the plot, we establish that scattered photons with

few events (i.e. snake photons) are the main competing process. The latter assertion is valid, because such photons maintain a propagation direction similar to that of ballistic radiation. Furthermore, the weight of such scattered radiation is significant, as opposed to that of highly diffuse photons.

Divergence of optical noise is fairly gradual. For the plots of Fig. 2, the observation plane is located 150 mm away from the sample. Despite such distant position, in highly forward-directed samples, scattered contributions overwhelm the signal of interest. In addition, snake photons do not suffer an important phase delay. Thus ballistic techniques which employ coherence gating [3,4], or ultra-fast imaging [15-18], encounter challenges while dealing with such radiation. To further validate this assertion, we acknowledge that the information in Fig. 2 is restricted to a path-length difference of 100 μm . Nonetheless, the influence of optical noise is orders of magnitude greater than the signal of interest.

The central purpose of this work is to present the theoretical foundation of a novel filter for selectively probing turbid media with ballistic photons. This is addressed in the second section. In the auto-correlation arrangement of Fig. 1, the filter would be used to couple exclusively ballistic light into the interferometer. We investigate the application range of the filter by evaluating samples with increasing anisotropy factors. Different configurations of the filter are considered, in order to counteract optical noise. For this purpose, in the third part of this work, we employ random walk Monte Carlo calculations, ray trace analysis, and conical diffraction theory of ruled gratings. Finally, in the last section, we conclude and present plausible future research directions.

Theory

In the introduction, we have emphasized that ballistic photons are commingled with forward-scattered ones. In addition, we have highlighted the intricacies associated with the separation of signal from noise. These difficulties arise because snake photons travel aside the ballistic component.

A characteristic feature of snake photons is the change in propagation direction that ensues after scattering. In the limiting case of single scattering, the radiation indisputably modifies its propagation direction. Hence, a filtering device that is sensitive to such angular variations could be optimal to isolate the faint signal of interest. In addition, a desirable feature of any system is simplicity of implementation. Taking these considerations into account, we suggest the use of

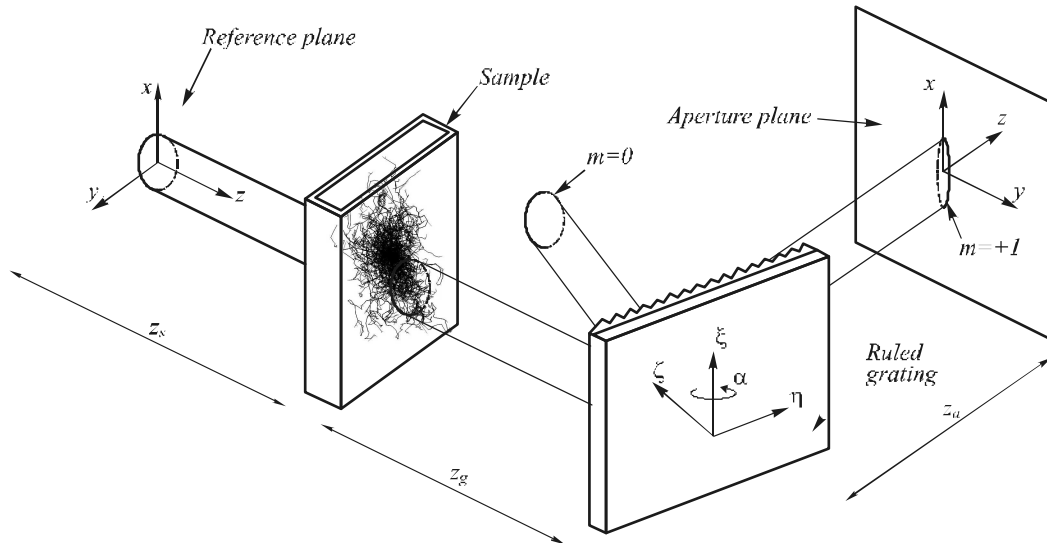


Fig. 3. In the angular filter, a ruled grating is positioned at grazing diffraction and a narrow aperture is used to block scattered light

In order to describe the behavior of the angular filter, we resort to the theory of conical diffraction of ruled gratings [19,20]. This approach is necessary because photons emerging from the sample exhibit random propagation directions. Thus, the radiation impinging on the diffractive element may not be perpendicular to the grooves. Propagation vectors \mathbf{k} of incident and diffracted beams are related as shown next.

$$k_{d\xi} = k_{i\xi} \quad (1)$$

$$k_{d\eta} = k_{i\eta} + 2\pi Gm \quad (2)$$

$$k_{d\zeta} = \sqrt{|\mathbf{k}|^2 - k_{d\xi}^2 - k_{d\eta}^2} \quad (3)$$

Here, $k_{i\xi}$ and $k_{d\xi}$ refer to the ξ component of incident and diffracted propagation vectors. For η and ζ , similar notations apply. G denotes groove frequency, and the media before and after diffraction is air.

From Eqs. (1) – (3), we may identify important features of the regime of operation. First, deviations in propagation direction are amplified non-linearly by the configuration. Second, certain photons will not propagate. The former feature is more easily ascertained for

a ruled diffraction grating, in conjunction with a narrow slit, as filtering device. The peculiarity of our proposal resides in the regime of operation of the diffractive element. The grating is positioned such that one of the first diffraction orders, $m = +1$, occurs at a grazing angle, as shown in Fig. 3.

In Fig. 3, the position of the diffractive element is determined by α . The direction of the optical axis is identical to the propagation direction of ballistic photons. z_s corresponds to the separation between the reference coordinate system and the sample. In the media, the traversed optical distance is random. The distance between sample and grating is z_g . In addition, z_u represents the separation between the grating and the aperture. The plane of the latter is taken as the observation plane.

in-plane diffraction; i.e. $k_{i\xi} = 0$. For such case, Eq. (2) may be rewritten in a familiar form.

$$\sin \beta = \sin \alpha + Gm\lambda \quad (4)$$

Here, incidence and diffracted angles are α and β , respectively. Meanwhile, λ is wavelength. In contrast to common applications of diffraction gratings, for the angular filter, the radiation is monochromatic. However, slight variations in incidence angle $\Delta\alpha$ occur. These deviations are a consequence of the random interactions of radiation with the turbid medium. For ballistic transillumination, we are especially interested in suppressing such contributions. The diffractive element provides an efficient and simple approach for this purpose. Variations in incidence angle are amplified, as shown in Eq. (5), by the grating. In Eq. (5), we omit the sign of the amplification term, which is in parentheses.

$$\Delta\beta = \left(\frac{\cos \alpha}{\cos \beta} \right) \Delta\alpha \quad (5)$$

From Eq. (5), we ascertain that angular deviations in the beam are augmented non-linearly. This is especially evident for near grazing diffraction, $\beta \rightarrow \pi/2$ [rad]. In the vicinity of such condition, certain photons will fail

to propagate. This feature is a direct consequence of the filter configuration.

In order to establish the degree of amplification of the system, we compute the expression in Eq. (5). We place particular emphasis on describing the behavior of the system in increments of 1 arc min. This analysis is important because, in the experiment, we employ a rotation scheme with such resolution [21].

In Fig. 4, we consider $G = 1200$ [lines/mm], $m = +1$, and $\lambda = 632.8$ [nm]. We depict a series of values with 1 arc min spacing. The first of such points occurs at an incidence angle of 13.8° (in the convention of Fig. 3, α is negative). We omit incidence angles below this threshold, because angular amplifications lie close together. Noteworthy is the rather steep increment in angular amplification. A rotating scheme with 1 arc min resolution allows a set of seven steps, with increasing angular amplification. Nonetheless, more sophisticated schemes may be used to explore the highly non-linear regime. Recently, this approach has served to improve spaceborne angular sensors [22,23].

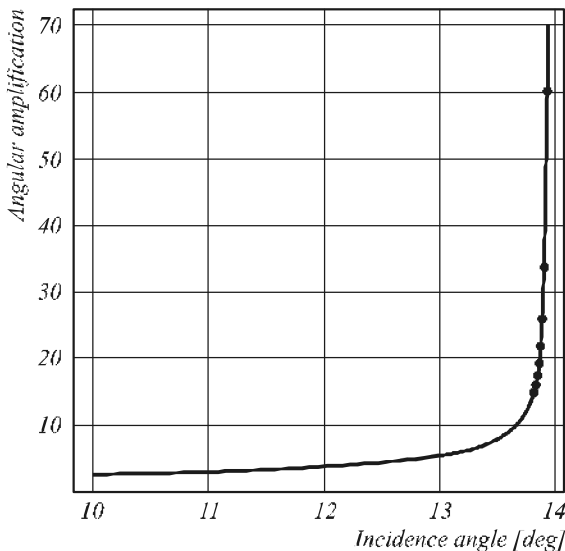


Fig. 4. Theoretical response of the system as the condition of grazing diffraction is approached. Starting at $15X$, points are separated 1 arc min

In terms of ballistic transillumination, higher amplification values are positive for discrimination purposes. This assertion is further validated by observing Fig. 3. In such figure, we notice a reduction in the transversal size of the diffracted beam. A direct inspection of the geometry reveals that incident and diffracted beams are related by the factor in parentheses of Eq. (5). Thus not only scattered light is deviated, also the area of interest is reduced substantially.

In order to assess the degree of filtering of the system, we emulate the interactions in the turbid medium with Monte Carlo (MC) computations. In previous publications, we have validated and employed the MC procedure in alternative transillumination modalities [24]. In addition, we propagate the radiation in homogenous media by utilizing ray trace methods. We use a reliable approach for this purpose [25].

We consider the radiation impinging on the sample to be collimated. Thus, the starting direction \mathbf{k}_0 is collinear to the optical axis. Incident propagation vectors \mathbf{k}_i are determined from the stochastic calculations. However, the reference coordinate system is different from that of the diffractive element. Hence, we perform a vector transformation and apply the expressions of conical diffraction theory. After grating interaction, we calculate \mathbf{k}_a and propagate the photons to the filter plane. The coordinate system at the observation (i.e. filter) plane is determined by the direction of ballistic photons. In Fig. 5, we illustrate the vector transformations required in the analysis.

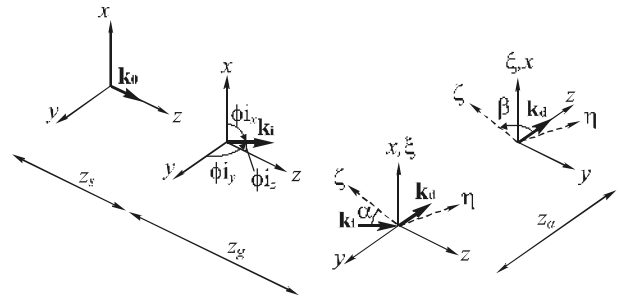


Fig. 5. Vector transformations needed to calculate the direction of propagation after conic diffraction

From the computations, we establish the extent of filtering. We determine the semi-minor and semi-major axes of the elliptic spatial distribution, and discard the photons outside such area. With this idea in mind, we now examine the performance of the filter.

Results and Discussion

An important topic that we are addressing is the extent of filtering, as the anisotropy factor increases. Experimentally, we have obtained encouraging results [21]. Nevertheless, a quantitative analysis of the extent of filtering has not been performed. The first feature to consider in the analysis is the sample under test. In Table 1, we describe the characteristics of the medium, which is comparable to dental enamel.

Table 1. Summary of Optical Properties

Model	μ_a [mm^{-1}]	μ_s [mm^{-1}]	g^*
(1)	0	0.591	0.93
(2)	0	0.591	0.99
(3)	0	0.591	0.995

* We utilize the Henyey-Greenstein phase function.

The second feature required in the study is the configuration of the filter. The random medium is located $z_s = 1$ [mm] away from the reference plane. The sample is contained in a recipient with 1 mm thick walls, and refractive index of 1.515. The thickness of the turbid medium is 10 mm, and the grating is located $z_g = 50$ [mm] away from the sample. The diffractive element is the same as the one alluded to earlier; $G = 1200$ [lines/mm], $m = +1$, and $\lambda = 632.8$ [nm]. Three arrangements, with increasing amplification, are studied. These configurations are described in Table 2.

Table 2. Configurations of the Angular Filter*

Incidence angle [deg]	Diffraction angle [deg]	Angular amplification
13.8000	86.2804	15.0
13.8833	87.8648	26.0
13.9167	89.0776	60.3

* Values are for ballistic photons.

From theory, we acknowledge that the values of angular amplification are constant exclusively for ballistic photons. In contrast, the angular increments of scattered radiation behave non-linearly. Some photons will fail to propagate, whereas others will diverge notably. The extent of divergence is related to the position of the plane of the aperture. A distant observation plane implies greater spatial departures for scattered photons. However, another relevant aspect concerns the collimation of ballistic radiation. The direction of propagation for unscattered radiation must be maintained. We, therefore, assess two positions for the observation plane, z_a : (i) 50 mm and (ii) 100 mm. These values are measured from the grating coordinate system, in the direction of the ballistic component. As reference scenario, shown in Fig. 6, we take model (2).

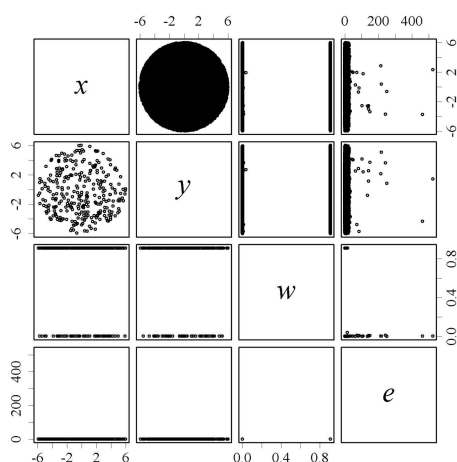


Fig. 6. In the reference scenario no filtering is considered, and the distance to the observation plane is 150 mm

The reference information is the same as the one depicted in model (2) of Fig. 2. However in the reference scenario of Fig. 6, no optical path-length restriction is considered. In order to separate the faint signal of interest, we suggest the implementation of the angular filter. In Fig. 7, we present the results for the filter in a 15X configuration. The response of the system is arranged similarly to the previous representations. The model number is located on the upper left corner. In addition, for the first row of depictions, the distance to the observation plane is 50 mm. For the second row, the separation is 100 mm. The location identifier is found on the lower right of each set of representations.

From Fig. 7, we recognize the behavior of the filter as predicted from theory. The spatial distribution of ballistic photons exhibits an elliptic form. The semi minor axis is reduced significantly $\sim 15X$. In addition, for $g \leq$

0.93, the angular filter enables perfect separation of signal from noise. For the observation plane located at 50 mm, we notice the presence of a few scattered photons. These particles have suffered multiple interactions and do not exhibit significant weights. Whenever the aperture plane is located farther away, we ascertain perfect isolation of the signal. Nevertheless, the location of the observation plane is of secondary importance for samples with $g \leq 0.93$.

The scenarios in (2) and (3) may be compared more fairly with the reference information. For samples with marked forward-directed scattering, the filter enables significant reduction of noise. In Fig. 6, optical noise is orders of magnitude greater than the signal. However after the implementation of the diffractive filter, the signal contributes more than the noise. The latter is irrespective of the value of the anisotropy factor. Nonetheless, for $g = 0.995$, optical noise is somewhat more intricate to overcome. In contrast, for $g = 0.99$ a 15X filter configuration enables near perfect signal isolation. This assertion is valid, provided that the filter plane is located 100 mm away from the sample.

The presence of multiply scattered light is also recognizable for samples with highly forward-scattering. However, the significance of such photons is negligible. If we discard the contributions of multiply scattered light, we observe that snake photons remain the major competing process. In samples with highly forward-scattering, photons that suffer few attenuation events retain significance and a similar propagation direction. In order to minimize the contributions of such snake photons, we may increase the filtering scheme to 26X. In Fig. 8, we show the response of the filter for such configuration.

We have shown that the filter effectively isolates ballistic photons for $g \leq 0.93$. Thus, in Fig. 8, we concentrate exclusively on samples with greater anisotropy values. For the configuration in Fig. 8, the semi minor axis of the elliptic distribution is $\sim 26X$ smaller than the reference value. Furthermore, angular variations in the beam are amplified by the same amount. Thus, we may estimate the filtering of optical noise by taking into consideration, independently, the angular amplification and the reduction of beam size. For the current arrangement, this yields a $26^2 \sim 675X$ filtering scheme. This value, however, is dependent on other features of the system.

The first factor has to do with the impediment of some photons to propagate. Certain scattered contributions will fail to continue after interacting with the grating. This behavior is an advantage of the configuration for the present application.

The second feature concerns the location of the aperture plane. Both, angular amplification and beam size reduction, affect the spatial location of photons after interaction. Therefore, if the aperture plane is located immediately after the diffractive element, we expect a more modest filtering scheme. In contrast, we anticipate a better performance of the system, whenever the aperture is located farther away.

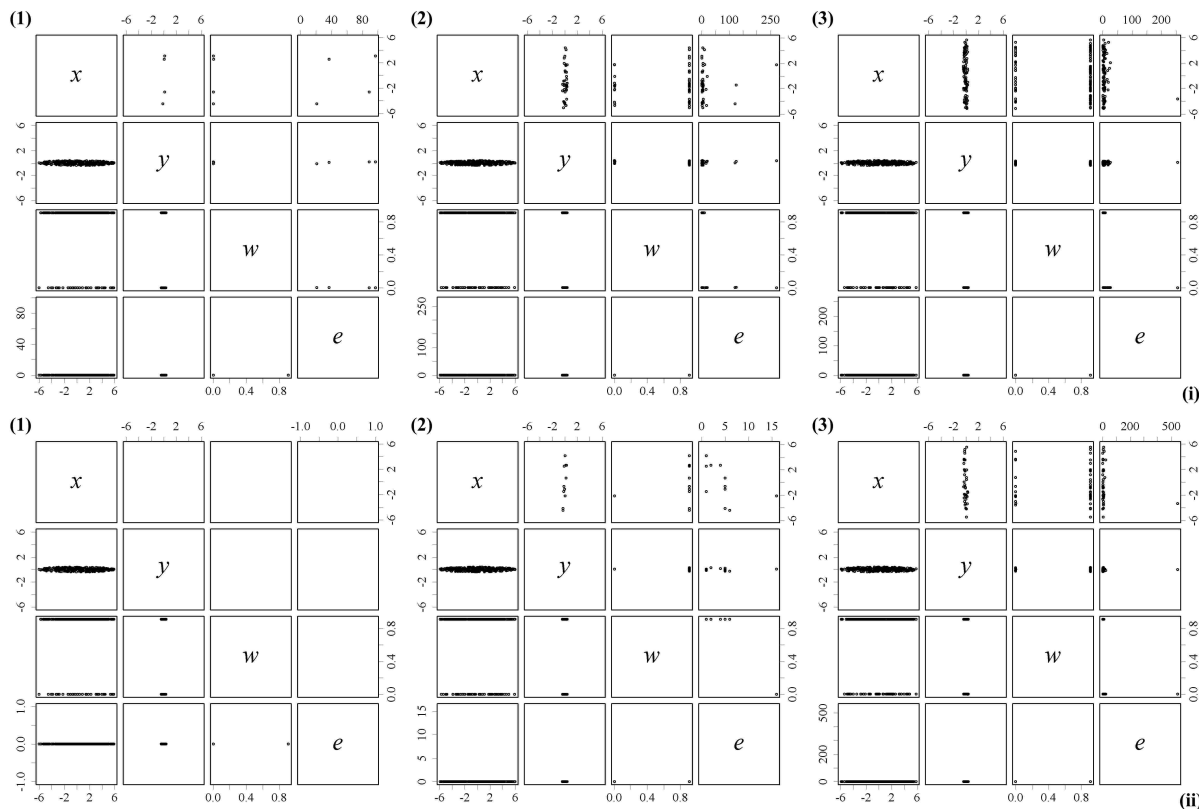


Fig. 7. The filter in a 15X configuration isolates ballistic photons for samples with $g \leq 0.93$. A greater distance to the observation plane, (i) 50 mm and (ii) 100 mm, is recommendable to enable spatial divergence of scattered photons

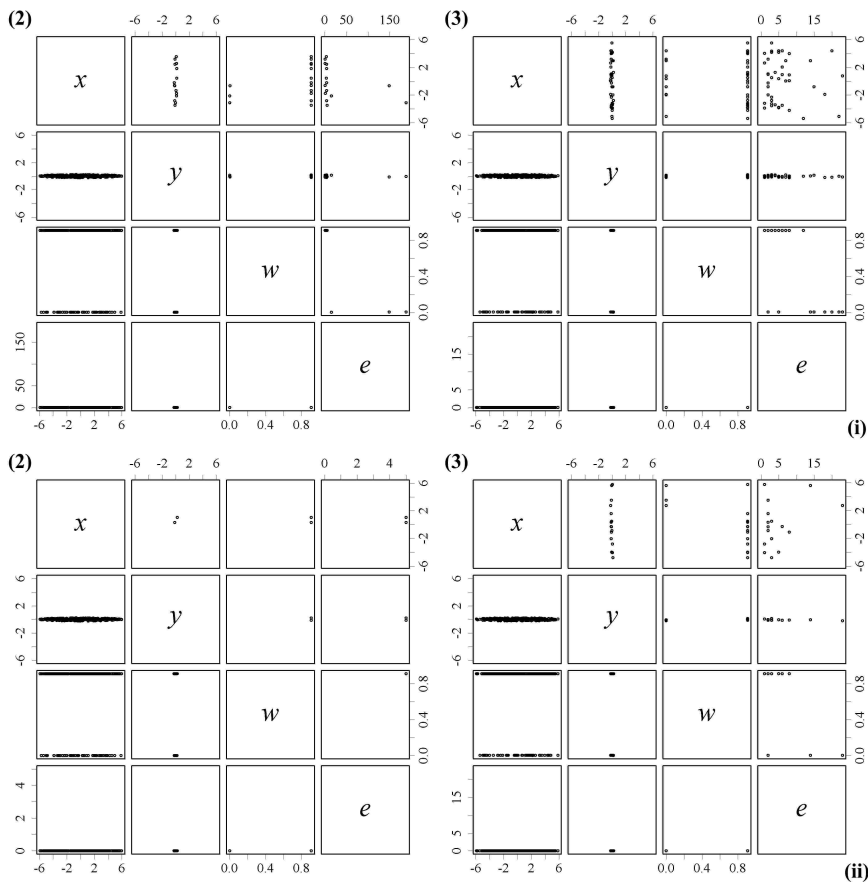


Fig. 8. The filter in a 26X configuration isolates ballistic photons for samples with $g \leq 0.99$

Table 3. Filtering of Scattered Photons for a 26X Configuration*

Model	Noise without filter**			Noise with filter			Noise reduction		
	(o)	(i)	(ii)	(o)	(i)	(ii)	(o)	(i)	(ii)
(2)	38263.8	20433.0	12490.9	87.499	10.936	1.821	437	1868	6859
(3)	54412.7	36096.4	25794.5	212.374	30.974	11.842	256	1165	2178

* Noise values are given in weight units, as determined from Monte Carlo (MC) computations. We assess 10^5 particles in MC calculations.

**The observation plane is separated from the grating (o) 1 mm, (i) 50 mm, and (ii) 100 mm.

From Monte Carlo calculations, we determine the behavior of forward-scattered particles. More specifically, we compute spatial distributions, significances, and propagation directions. Thus, we may calculate the amount of scattered photons in the reference scenarios (such as Fig. 6), and after the diffractive filter. From the ratio of these values, we may determine the extent of filtering. In Table 3, we present this analysis for three distances to the aperture plane (o) 1 mm, (i) 50 mm, and (ii) 100 mm.

From the values in Table 3, we ascertain that the filter enables significant reduction of scattered radiation. In fact, for $g \leq 0.99$, the angular filter in a 26X configuration enables isolation of signal from noise. For very marked forward-scattering $g \geq 0.995$, we may employ the filter in a 60X configuration. As in the previous arrangement, this yields a filtering scheme of $60^2 \sim 3600X$. Here, we consider the contributions of angular amplification and beam size reduction to be independent. However, as discussed before, we expect deviations from this value. In Fig. 9 and Table 4, we present the response of the system for a 60X configuration.

Table 4. Filtering of Noise for a 60X Arrangement*

Model	Noise reduction		
	(o)	(i)	(ii)
(3)	1270	4403	7079

* Refer to Table 3 for reference (Noise without filter) values.

The presence of snake photons remains the principal source of optical noise. In Fig. 9, the limiting case of single scattering is recognizable. This occurs when the observation plane is separated from the grating 100 mm. In addition, we ascertain a significant $\sim 10^3$ reduction of optical noise. Despite high anisotropies, we may recover the faint signal of interest.

The filter we have presented in this work may be implemented readily for applications involving tissue characterization. In our group, we are also interested in performing tissue imaging. Furthermore, we would like to complement the technique with interferometric methods. In fact, as mentioned in the introduction, we are interested in developing the proposal into an auto-correlation interferometer. For imaging applications, we foresee challenges due to the marked asymmetry of the spatial distribution.

In order to overcome such asymmetry, we may introduce a second diffractive element. Taking Fig. 3 as reference, we should position the additional grating in the aperture plane. The grooves need to be parallel to the y axis, and by rotating the element we should reach the grazing diffraction condition. An advantage of this configuration is that the angular amplification occurs in a transversal direction. In addition, if the characteristics

of the gratings match, we anticipate that the spatial asymmetry will be removed. This behavior implies, in turn, that conventional diaphragms could be used instead of slits to block scattered light.

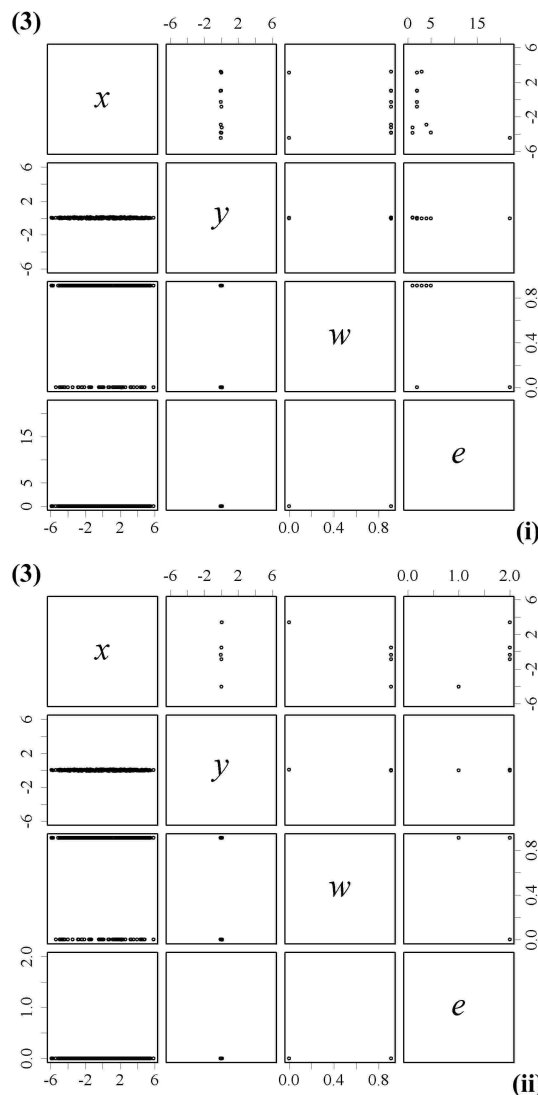


Fig. 9. The filter in a 60X arrangement provides a reduction of optical noise of $\sim 10^3$ for $g \geq 0.995$

As an example, consider a circular aperture with a diameter of 12 mm, and diffractive elements in a 15X configuration; with $G = 1200$ [lines/mm], $m = +1$, and $\lambda = 632.8$ [nm]. The filtered distribution would retain the circular pattern, but with a diameter of 800 μm . Radiation from this configuration could then be used as input to a ballistic auto-correlation interferometer. By removing the asymmetry, the system could be employed for imaging and characterization of tissues with ballistic photons.

The analysis presented in this work does not take into account the decrease in signal due to (grazing) diffraction. Such behavior affects both ballistic and forward-scattered contributions. The undertaking of this analysis would complement the calculations presented herein. Nonetheless, as a result of this work, we assert that solely the effects of ballistic radiation need be considered.

Conclusions and Future Work

The utilization of a non-linear grating-based angular filter enables the separation of ballistic photons from those that have undergone scattering. The suggested system is conformed by a monochromatic source incident on a ruled grating, positioned at grazing diffraction, followed by a narrow slit.

Despite large spatial extents and highly forward-directed scattering ($g > 0.9$), angular amplification and beam size reduction permit isolated detection of the signal of interest. Minute deviations in propagation angle of scattered radiation are amplified non-linearly. A rotation scheme with 1 arc min resolution may provide angular amplifications in the range of 15X-60X. In addition, similar values of transversal beam size reduction enable efficient $\sim 100\text{X}$ - 1000X filtering of scattered photons.

In the transillumination procedure, the filter provides a scheme to significantly reduce optical noise. By using random walk Monte Carlo calculations, ray trace analysis, and conical diffraction theory of ruled gratings, we assessed the behavior of the system as the anisotropy increases. For samples with $g \leq 0.99$, the filter enables isolation of ballistic photons. In addition for very marked forward-scattering $g \geq 0.995$, the configuration permits a significant $\sim 10^3$ reduction of optical noise.

Our future research efforts will be focused on the implementation of a ballistic auto-correlation interferometer. For this purpose, we will investigate the use of a 2D grating-based scheme as filter and coupler.

Acknowledgments

Paulino Vacas-Jacques gratefully acknowledges the National Science and Technology Council of Mexico (CONACyT) for the financial support assigned to collaborate at Saratov State University, grant 172068. The same author thanks the "Centro de Investigaciones en Optica" for partial funding of travel expenses.

This research was performed in the framework of the project "Applications of infrared interferometry for biomedical tomography" (CONACyT 2007-I0003-60450), and of the Russian Federation Program for the Development of High School Potential (2009-2010), projects № 2.1.1/4989 and № 2.2.1.1/2950.

References

1. Diagnosis and management of dental caries throughout life / National Institutes of Health Consensus Statement 18: NIH, 2001. - 30 p.
2. **Bühler, C.** Imaging of occlusal dental caries (decay) with near-IR light at 1310-nm / C. Bühler, P. Ngaotheppitak, D. Fried // *Opt. Express* 2005. Vol. 13. P. 573-582.
3. **Vacas-Jacques, P.** Pass-through photon-based biomedical transillumination / P. Vacas-Jacques, G. Paez, M. Strojnik // *J. Biomed. Opt.* 2008. Vol. 13. P. 041307.
4. **Vacas-Jacques, P.** Forward-calculated analytical interferograms in pass-through photon-based biomedical transillumination / P. Vacas-Jacques, M. Strojnik, G. Paez // *J. Opt. Soc. Am. A* 2009. Vol. 26. P. 602-612.
5. **Лычагов, В.В.** Автокорреляционная низкокогерентная интерферометрия рассеивающих и слоистых объектов / В.В. Лычагов, Д.В. Лякин, М.Д. Модель, В.П. Рябухо // *Компьютерная оптика*. 2007. Т.31. №3. С. 40-51.
6. **Modell, M.** Autocorrelation low coherence interferometry / M. Modell, V. Ryabukho, D. Lyakin, V. Lychagov, E. Vitkin, I. Itzkan, L.T. Perelman // *Opt. Commun.* 2008. Vol. 281. P. 1991-1996.
7. **Chang, J.** Imaging of fluorescence in highly scattering media / J. Chang, H. Graber, R. Barbour // *IEEE Trans. Biomed. Eng.* 1997. Vol. 44. P. 810-822.
8. **Graaff, R.** Diffusion coefficient in photon diffusion theory / R. Graaff, J.J. Ten Bosch // *Opt. Lett.* 2000. Vol. 25. P. 43-45.
9. **Kim, A.D.** Transport theory for light propagation in biological tissue / A.D. Kim // *J. Opt. Soc. Am. A* 2004. Vol. 21. P. 820-827.
10. **Kim, A.D.** Radiative transport theory for optical molecular imaging / A.D. Kim, M. Moscoso // *Inverse Probl.* 2006. Vol. 22. P. 23-42.
11. **Flock, S.T.** Total attenuation coefficients and scattering phase functions of tissues and phantom materials at 633 nm / S.T. Flock, B.C. Wilson, M.S. Patterson // *Med. Phys.* 1987. Vol. 14. P. 835-841.
12. **Cheong, W.F.** A review of the optical properties of biological tissues / W.F. Cheong, S.A. Prahl, A.J. Welch // *IEEE J. Quantum Elect.* 1990. Vol. 26. P. 2166-2185.
13. Optical-thermal response of laser-irradiated tissue: Summary of optical properties / W.F. Cheong; A.J. Welch (ed.) // Plenum Press, New York, 1995, Appendix. Chap. 8.
14. **Fried, D.** Early caries imaging and monitoring with near-infrared light / D. Fried, J. Featherstone, C. Darling, R. Jones, P. Ngaotheppitak, C. Bühler // *Dent. Clin. North Am.* 2005. Vol. 49. P. 771-793.
15. **Wang, L.** Ballistic 2-D imaging through scattering walls using an ultrafast optical Kerr gate / L. Wang, P. Ho, C. Liu, G. Zhang, R. Alfano // *Science* 1991. Vol. 253. P. 769-771.
16. **Hee, M.** Femtosecond transillumination tomography in thick tissues / M. Hee, J. Izatt, E. Swanson, J. Fujimoto // *Opt. Lett.* 1993. Vol. 18. P. 1107-1109.
17. **Le Tolguenec, G.** Two-dimensional time-resolved direct imaging through thick biological tissues: a new step toward noninvasive medical imaging / G. Le Tolguenec, F. Devaux, E. Lantz // *Opt. Lett.* 1998. Vol. 24. P. 1047-1049.
18. **Yasui, T.** Ultrafast time-resolved spectroscopic imaging using femtosecond amplifying optical Kerr gate / T. Yasui, E. Abraham, K. Minoshima, H. Matsumoto, G. Jonusauskas, C. Rulliere // *Nonlinear Optics '98: Materials, Fundamentals and Applications Topical Meeting* 1998. P. 218-220.
19. **Popov, E.** Conical diffraction mounting generalization of a rigorous differential method / E. Popov, L. Mashev // *J. Optics* 1986. Vol. 17. P. 175-180.
20. **Loewen E.G.** Diffraction gratings and applications / E.G. Loewen, E. Popov - New York: Dekker, 1997. - 601 p.

21. **Vacas-Jacques, P.** Non-linear grating-based angular filter for ballistic transillumination / P. Vacas-Jacques, V.P. Ryabukho, M. Strojnik, V.V. Tuchin, G. Paez // Accepted for presentation in: European Conferences on Biomedical Optics 2009.
22. **Sun, K.X.** Grating angle magnification enhanced angular and integrated sensors for LISA applications / K.X. Sun, S. Buchman, R. Byer // J. Phys.: Conf. Ser. 2006. Vol. 32. P. 167-179.
23. **Sun, K.X.** Grating angle magnification enhanced angular sensor and scanner / K.X. Sun, R. Byer // United States Patent No. 20080002197A1, Palo Alto, 2008, Appl. No. 11/820,720.
24. **Vacas-Jacques, P.** Monte-Carlo simulation of photon trans-illumination time of flight / P. Vacas-Jacques, M. Strojnik, G. Paez // Proc. SPIE, 2007. Vol. 6631. P. 663114-1-663114-12.
25. **Gutierrez-Herrera, E.** Interferometric tolerance determination for a Dove prism using exact ray trace / E. Gutierrez-Herrera, M. Strojnik // Opt. Commun. 2008. Vol. 281. P. 897-905.

ТЕОРЕТИЧЕСКИЙ АНАЛИЗ ДЕЙСТВИЯ ДИФРАКЦИОННОГО ФИЛЬТРА В МЕТОДЕ БАЛЛИСТИЧЕСКОГО ПРОСВЕЧИВАНИЯ РАССЕИВАЮЩИХ СРЕД

Паулино Вакас-Жакс¹ (аспирант, e-mail: pvj@cio.mx),
 Владимир Петрович Рябухо^{2,3} (профессор кафедры, e-mail: rvp@sgu.ru),
 Мария Стройник¹ (профессор, e-mail: mstrojnik@aol.com),
 Валерий Викторович Тучин^{2,3} (заведующий кафедрой, e-mail: tuchin@sgu.ru),
 Гонзало Паез¹ (профессор, e-mail: gpaez@cio.mx)

¹ Centro de Investigaciones en Optica, 37000, Leon, Guanajuato, Mexico

² Саратовский государственный университет,

³ Институт проблем точной механики и управления РАН

Аннотация

Обсуждается метод селективной регистрации баллистических фотонов при исследовании мутных сред, подобных биологическим тканям. Рассматриваются среды с сильным анизотропным рассеянием вперед (коэффициент анизотропии $g > 0,9$). Предложено применение дифракционного нелинейного фильтра углового спектра оптических волн для отделения слабого баллистического сигнала от оптического шума, обусловленного рассеянием вперед. Для реализации фильтрации используется отражающая дифракционная решетка и пространственная фильтрация монохроматического дифрагированного излучения с помощью узкой щели в скользящих дифракционных порядках. Малые отклонения в углах распространения рассеянного излучения нелинейно увеличиваются в дифрагированном излучении. Поворотная схема фильтрации с разрешением в 1 угловую минуту обеспечивает угловое увеличение в 15-60 раз. Кроме этого, поперечное сокращение апертуры дифрагированного пучка обеспечивает эффективную 100-1000 кратную фильтрацию оптического шума. Выполнены расчеты по методу Монте-Карло для имитирования взаимодействия оптического излучения с мутной средой. Влияние фильтра рассматривается путем использования лучевого анализа и теории конической дифракции на отражающей дифракционной решетке. Для образцов с $g \leq 0,99$ продемонстрировано, что фильтр позволяет изолировать баллистические фотоны. Для сильно анизотропного рассеяния вперед, $g \geq 0,995$, схема фильтрации обеспечивает существенное ($\sim 10^3$) снижение оптического шума.

Ключевые слова: пространственно-угловой фильтр, скользящая дифракция, отражающие дифракционные решетки, коническая дифракция, метод Монте-Карло, баллистическое просвечивание, имиджинг и анализ биологических тканей.

В редакцию поступила 21.04.2009г.